

An External Inverse Compton Emission Model of Gamma-Ray Burst High-Energy Lags

K. Toma^{1,2}, X. F. Wu^{1,2,3}, and P. Mészáros^{1,2,4}

¹*Department of Astronomy and Astrophysics, Pennsylvania State University, 525 Davey Lab, University Park, PA 16802, USA*

²*Center for Particle Astrophysics, Pennsylvania State University, University Park, PA 16802, USA*

³*Purple Mountain Observatory, Chinese Academy of Sciences, Nanjing 210008, China and*

⁴*Department of Physics, Pennsylvania State University, University Park, PA 16802, USA*

The *Fermi* satellite has been reporting the detailed temporal properties of gamma-ray bursts (GRBs) in an extremely broad spectral range, 8 keV - 300 GeV, in particular, the unexpected delays of the GeV emission onsets behind the MeV emission of some GRBs. We focus on GRB 080916C, one of the *Fermi*-LAT GRBs for which the data of the delayed high-energy emission are quite extensive, and we show that the behavior of the high-energy emission of this burst can be explained by a model in which the prompt emission consists of two components: one is the MeV component due to the synchrotron-self-Compton radiation of electrons accelerated in the internal shock of the jet and the other is the high-energy component due to inverse Compton scattering of the photospheric X-ray emission of the expanding cocoon off the same electrons in the jet. Such an external inverse Compton effect could be important for other *Fermi*-LAT GRBs, including short GRBs as well. In this model, the delay timescale is directly linked to the physical properties of GRB progenitor.

1. Introduction

Gamma-ray bursts (GRBs) were only sparsely observed in the > 100 MeV range, until the *Fermi* satellite was launched on June 11 2008 [1]. Now *Fermi* provides extremely broad energy coverage, 8 keV – 300 GeV, with high sensitivity for GRBs, and is accumulating a wealth of new data which open a completely new window on the physics of GRBs. The high-energy temporal and spectral data provided by *Fermi* can severely constrain the physical parameters of the GRB emission region and the circumburst environment, which will lead to a deeper understanding of the central engine and the GRB progenitors, and will also constrain models of high-energy cosmic ray acceleration [2, 3].

GRB 080916C has the largest isotropic γ -ray energy release so far, $E_{\gamma, \text{iso}} \simeq 8.8 \times 10^{54}$ erg (with redshift $z \simeq 4.35$). *Fermi* LAT obtained its high-energy emission data quite extensively, showing several important new properties [4]:

- (i) The time-resolved spectra (with resolution ~ 5 – 50 s) are well fitted by a smoothly broken power-law function (the so-called Band function) from 8 keV up to a photon with energy ≈ 13.2 GeV.
- (ii) The $\varepsilon > 100$ MeV emission is not detected together with the first $\varepsilon \lesssim 1$ MeV pulse and the onset of the $\varepsilon > 100$ MeV emission coincides with the rise of the second pulse (≈ 5 s after the trigger).
- (iii) Most of the emission in the second pulse shifts towards later times as higher energies are considered.

- (iv) The $\varepsilon > 100$ MeV emission lasts at least 1400 s, while photons with $\varepsilon < 100$ MeV are not detected past 200 s.

Some other *Fermi*-LAT GRBs also display high-energy lags, similar to the properties (ii) and/or (iii) [4, 5], and then they should be very important to understand the prompt emission mechanism of GRBs. We will call the $\varepsilon \lesssim 1$ MeV emission and the $\varepsilon > 100$ MeV emission "MeV emission" and "high-energy emission", respectively.

A simple physical picture for the property (i) is that the prompt emission consists of a single emission component, such as synchrotron radiation of electrons accelerated in internal shocks of a relativistic jet. In this picture, the peak of the MeV pulse could be attributed to the cessation of the emission production (i.e., the shock crossing of the shell) and the subsequent emission could come from the high latitude regions of the shell. Thus the observed high-energy lag for the second pulse (property (iii)) requires that the electron energy spectrum should be harder systematically in the higher latitude region. This would imply that the particle acceleration process should definitely depend on the global parameters of the jet, e.g., the angle-dependent relative Lorentz factor of the colliding shells, but such a theory has not been formulated yet. The property (ii) could be just due to the fact that the two pulses originate in two internal shocks with different physical conditions for which the electron energy spectrum of the second internal shock is harder than that of the first one [4].

Another picture is that the prompt emission consists of the MeV component and a delayed high-energy component. The latter component could be produced by hadronic effects (i.e., photo-pion process and proton synchrotron emission) [6, 7], but they require ex-

tremely large total energy budget [8].

In this paper, we discuss a different two-component emission picture in which the delayed high-energy component is produced by leptonic process (i.e., electron inverse Compton scattering). We focus on the effect that the ambient radiation up-scattered by the accelerated electrons in the jet can have a later peak than that of the synchrotron and synchrotron-self-Compton (SSC) emission of the same electrons (corresponding to the property (iii)) [9, 10, 11]. Provided that the seed photons for the Compton scattering come from the region behind the electron acceleration region of the jet (see Figure 1), the up-scattered high-energy photon field is highly anisotropic in the comoving frame of the jet, i.e., the emissivity is much larger for the head-on collisions of the electrons and the seed photons. As a result, a stronger emission is observed from the higher latitude regions, and thus its flux peak lags behind the synchrotron and SSC emission.

Here we propose that the seed photons may be provided by the photospheric emission of an expanding cocoon. GRB 080916C is a long GRB, and it may originate from the collapse of a massive star. The relativistic jet produced in the central region penetrates the star and deposits most of its energy output into a thermal bubble, or cocoon, until it breaks out of the star [12, 13, 14, 15]. The cocoon can store an energy comparable or larger than the energy of the prompt emission of the jet, and thus it may make an observable signature outside the star [16, 17]. The cocoon escaping from the star will emit soft X-rays, and these can be up-scattered by the accelerated electrons in the jet into the high-energy range. The optical thinning of the expanding cocoon may be delayed behind the prompt emission of the jet, so that the onset of the high-energy emission is delayed behind the MeV emission (corresponding to the property (ii)). Thus this model has the potential for explaining the two delay timescales; the delayed onset of the high-energy photons (property (ii)) is due to the delayed emission of the cocoon, while the high-energy lag within the second pulse (property (iii)) is due to the anisotropic inverse Compton scattering. We also show that the combination of the time-averaged spectra of the SSC and the up-scattered cocoon (UC) emission is roughly consistent with the observed smooth power-law spectrum (property (i)) (see Figure 2).

As we will explain below, the UC emission is short-lived and may not account for the whole high-energy emission, which lasts much longer than the MeV emission (property (iv)). It is natural that the high-energy emission in later times is related to the afterglow, i.e., produced by the external shock which propagates in the circumburst medium. This possibility is studied by [18]. They claim that even the onset phase of the high-energy emission is produced by the external shock. However, the rise of the flux of GRB

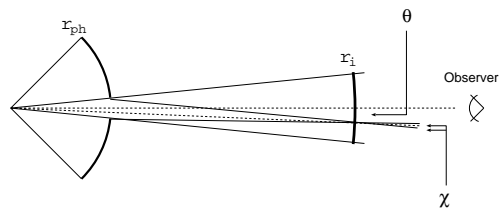


Figure 1: Geometry of our model. The jet with opening angle $\theta_j \simeq 0.01$ and the cocoon with opening angle $\theta_c \simeq 0.8$ are ejected from the collapsing star. The cocoon becomes optically thin at $r = r_{\text{ph}}$ some time ($\lesssim 5$ s) after the burst trigger. The second pulse of the prompt emission is produced by the accelerated electrons in the internal shock of the jet at $r = r_i$, and the cocoon X-ray photons are up-scattered by the same electrons at $r = r_i$ into the GeV range.

080916C in the LAT energy range ($\sim t^6$) is too steep for the external shock to reproduce it. Thus at least the first part of the delayed high-energy component of this burst should be related to the prompt emission.

Although we focus on GRB 080916C to examine whether the UC emission is viable for its properties in the high energy range in this paper, our modeling is generic, and the UC emission could be important for some other *Fermi*-LAT GRBs (including short GRBs). We will discuss the temporal and spectral properties of the cocoon emission (in § 2), the synchrotron and SSC emission of the jet (in § 3), and the UP emission of the jet (in § 4). We summarize our model and its implications in § 5. For more details, see [19].

2. Cocoon Emission

We take the total energy and the total mass of the cocoon and the stellar radius as parameters, E_c , M_c , and r_* , respectively. After the jet breaks out of the star, the cocoon expands with the sound speed, $c_s = c/\sqrt{3}$, where c is the speed of light. The cocoon expands by its own thermal pressure in the comoving frame as expected in the standard fireball model [2]. Its expansion speed in the comoving frame suddenly becomes close to c , and then the opening angle of the cocoon measured in the central engine frame is given by $\theta_c \simeq \Gamma_{c,\text{ex}}^{-1}$, where $\Gamma_{c,\text{ex}}$ is the Lorentz factor corresponding to c_s . Thus we obtain $\theta_c \simeq \sqrt{2/3} \simeq 0.8$. This rough estimate is consistent with the results of the numerical simulations [15].

The cocoon material accelerates as $\Gamma \propto r$ and reaches the terminal Lorentz factor $\Gamma_c = E_c/M_c c^2$ at $r_s = r_* \Gamma_c = 5.0 \times 10^{12} r_{*,11} (\Gamma_c/50)$ cm. (We adopt the notation $Q = 10^x Q_x$ in cgs units throughout this paper.) For $r > r_s$, the cocoon material is dominated by the kinetic energy. The radiation stored in the cocoon is released when the opacity for the electron scattering becomes less than unity. The photosphere

radius is given by

$$r_{\text{ph}} \simeq \left[\frac{E_c \sigma_T}{2\pi(1 - \cos\theta_c) \Gamma_c m_p c^2} \right]^{1/2} \\ \simeq 2.1 \times 10^{14} E_{c,52}^{1/2} \left(\frac{\Gamma_c}{50} \right)^{-1/2} \text{ cm}, \quad (1)$$

where σ_T is Thomson cross section.

The cocoon may become optically thin later than the onset of the first MeV pulse (i.e., the burst trigger time). Let $t = 0$ be the photon arrival time at the earth emitted at the stellar surface at the jet breakout. The first MeV pulse produced within the jet at $r = r_i$ is observed at $t \simeq \Delta t_i \equiv r_i(1+z)/(2c\Gamma_j^2)$, where Γ_j is the bulk Lorentz factor of the jet and z is the source redshift. This timescale is comparable to the angular spreading timescale of the pulse, and we can take $\Delta t_i \simeq 2$ s for GRB 080916C. The second MeV pulse is observed $\simeq 5$ s after the burst trigger, i.e., at $t \simeq \Delta t_i + 5 \simeq 7$ s. On the other hand, the cocoon photospheric emission is observed at

$$t \simeq \Delta t_c \equiv \frac{r_{\text{ph}}}{2c\Gamma_c^2} (1+z) \simeq 7.5 E_{c,52}^{1/2} \left(\frac{\Gamma_c}{50} \right)^{-5/2} \text{ s}, \quad (2)$$

where we have used $z \simeq 4.35$. The cocoon photospheric emission may be observed from $t = \Delta t_c$ to $t = \Delta t_c + \Delta t_d$, where $\Delta t_d \sim \Delta t_c$ is the time during which the cocoon will be adiabatically cooled. If internal dissipation occurs in the jet at $r = r_i > r_{\text{ph}}$ making the second MeV pulse within the duration of the cocoon emission, the cocoon photons may be up-scattered to higher energies by the energetic electrons within the dissipation region of the jet, which may be observed along with the second MeV pulse. Therefore we require a condition $\Delta t_i < \Delta t_c \lesssim \Delta t_i + 5$. This condition puts a constraint to the physical parameters of the cocoon,

$$0.3 < E_{c,52}^{1/2} \left(\frac{\Gamma_c}{50} \right)^{-5/2} \lesssim 0.9 \quad (3)$$

We adopt the parameters $E_c \simeq 10^{52}$ erg and $\Gamma_c \simeq 50$ for the purposes of calculating the flux of the cocoon emission.

The comoving temperature of the cocoon when its opening angle becomes θ_c is approximately given by $T'_{\text{init}} \simeq [E_c/(2\pi(1 - \cos\theta_c)r_*^3 a)]^{1/4}$, where a is the Stefan constant. Then the temperature at the photosphere is estimated to be $T'_{\text{ph}} = T'_{\text{init}}(r_s/r_*)^{-1}(r_{\text{ph}}/r_s)^{-2/3}$. Non-thermal electrons injected by internal shocks within the photosphere may make the emission be quasi-thermal. Its spectrum is written by

$$F_\varepsilon^{\text{co}} = F_{\varepsilon_{\text{ph}}}^{\text{co}} \times \begin{cases} \left(\frac{\varepsilon}{\varepsilon_{\text{ph}}^{\text{co}}} \right)^2 & \text{for } \varepsilon < \varepsilon_{\text{ph}}^{\text{co}}, \\ \left(\frac{\varepsilon}{\varepsilon_{\text{ph}}^{\text{co}}} \right)^\beta & \text{for } \varepsilon_{\text{ph}}^{\text{co}} < \varepsilon < \varepsilon_{\text{cut}}^{\text{co}}, \end{cases} \quad (4)$$

where $\varepsilon_{\text{ph}}^{\text{co}}$ and $F_{\varepsilon_{\text{ph}}}^{\text{co}}$ are given by

$$\varepsilon_{\text{ph}}^{\text{co}} \simeq 2.82 kT'_{\text{ph}} \frac{2\Gamma_c}{1+z} \simeq 1.2 E_{c,52}^{-1/12} r_{*,11}^{-1/12} \text{ keV} \left(\frac{\Gamma_c}{50} \right) \quad (5)$$

$$F_{\varepsilon_{\text{ph}}}^{\text{co}} \simeq \frac{(1+z)^3}{d_L^2} \frac{2\pi(\nu_{\text{ph}}^{\text{co}})^2}{c^2} kT'_{\text{ph}} \Gamma_c \left(\frac{r_{\text{ph}}}{\Gamma_c} \right)^2 \\ \simeq 31 E_{c,52}^{3/4} r_{*,11}^{-1/4} \text{ keV cm}^{-2} \text{ s}^{-1} \text{ keV}^{-1}, \quad (6)$$

where $\nu_{\text{ph}}^{\text{co}} = \varepsilon_{\text{ph}}^{\text{co}}/h$ (h is the Planck constant), and we have taken the luminosity distance of GRB 080916C as $d_L \simeq 1.2 \times 10^{29}$ cm. Some numerical calculations of the radiative processes in the cocoon show $\beta \sim -1$ and $\varepsilon_{\text{cut}}^{\text{co}} \sim 30 \times \varepsilon_{\text{ph}}^{\text{co}}$ [17].

The observation of GRB 080916C shows that there is no excess from the Band spectrum at the X-ray band, $\gtrsim 10$ keV, and we obtain a rough upper limit of the cocoon X-ray emission $\varepsilon_{\text{ph}}^{\text{co}} F_{\varepsilon_{\text{ph}}}^{\text{co}} \lesssim 40 \text{ keV cm}^{-2} \text{ s}^{-1}$. This limit leads to another constraint on the cocoon parameters,

$$r_{*,11} \gtrsim 0.8 E_{c,52}^2 \left(\frac{\Gamma_c}{50} \right)^3. \quad (7)$$

3. Synchrotron and SSC Emission

We can constrain, from the *Fermi* observation, the global physical parameters of the jet: the bulk Lorentz factor Γ_j , the emission radius of the second pulse r_i , and the opening angle θ_j . First of all, from the absence of a $\gamma\gamma$ absorption cutoff, we obtain a lower limit on the bulk Lorentz factor of the jet, $\Gamma_j \gtrsim 870$ [4]. Since the angular spreading timescale of the pulse is $\Delta t_i \simeq 2$ s for the second pulse, similar to the first pulse, the emission radius is estimated by

$$r_i \simeq 2c\Gamma_j^2 \frac{\Delta t_i}{1+z} \simeq 2.2 \times 10^{16} \Gamma_{j,3}^2 \left(\frac{\Delta t}{2 \text{ s}} \right) \text{ cm}. \quad (8)$$

Since GRB 080916C is so bright, it is probable that the jet is viewed on-axis, and we adopt this assumption as a simplification (see Figure 1). In this case, the cocoon is viewed off-axis, since the jet cone will not be filled with the cocoon material. The cocoon emission is thus less beamed, but this off-axis effect is not significant because the opening angle of the jet can be estimated to be small. The isotropic γ -ray energy of this burst is 8.8×10^{54} erg. To obtain a realistic value of the collimation-corrected γ -ray energy, $\lesssim 10^{51}$ erg, the jet opening angle is constrained by $\theta_j \lesssim 0.015$. We adopt $\theta_j \simeq 0.01$, and having adopted a nominal value of $\Gamma_c \simeq 50$ in accord with the observed time delay of the high-energy emission (equation 3), we obtain

$$\Gamma_c \theta_j \simeq 0.5 < 1. \quad (9)$$

Thus the off-axis dimming and softening effects are not significant for the cocoon emission.

We assume that the jet is dominated by the kinetic energy of protons and we estimate the physical parameters of the jet dissipation region for the second MeV pulse. In the scenario where the dissipation is due to internal shocks [2], the collisionless shock waves can amplify the magnetic field and accelerate electrons to a power-law energy distribution, which then produce synchrotron radiation and SSC radiation. At $r = r_i$, the comoving number density of the jet is estimated by $n' = L\Delta t_i / (4\pi r_i^3 m_p c^2 (1+z))$, where L is the isotropic-equivalent luminosity of the jet. The internal energy density produced by the internal shock is given by $u' = n'\theta_p m_p c^2$, where θ_p is a factor of order unity. Assuming that a fraction ϵ_B of the internal energy of the protons is carried into the magnetic field, the field strength is estimated by $B' = (8\pi\epsilon_B u')^{1/2}$. Assuming that a fraction ϵ_e of the internal energy of the protons is given to the electrons, the minimum Lorentz factor of the electrons is given by $\gamma_m = [(p-2)/(p-1)](m_p/m_e)\epsilon_e\theta_p$, where p is the index of the electron energy distribution and we have assumed that it is similar to the value inferred from the spectrum of the first pulse, $p \simeq 3.2$. We find that the cooling electron Lorentz factor $\gamma_c \sim \gamma_m$ for fitting the observational data. In this case we obtain $\gamma_c \simeq 360(\epsilon_B/10^{-5})^{-1/3}(\tau/4 \times 10^{-4})^{-2/3}$, where $\tau = \sigma_T n' r_i / \Gamma_j$ is the Thomson optical depth.

The synchrotron characteristic energy and the synchrotron peak flux (at the synchrotron energy corresponding to γ_c) are estimated by

$$\begin{aligned} \varepsilon_m &\simeq \frac{3heB'}{4\pi m_e c} \gamma_m^2 \frac{2\Gamma_j}{1+z} \simeq 2.7 L_{55}^{1/2} \Gamma_{j,3}^{-2} \left(\frac{\Delta t_i}{2 \text{ s}}\right)^{-1} \\ &\times \theta_p^{5/2} \left(\frac{\epsilon_B}{10^{-5}}\right)^{1/2} \left(\frac{\epsilon_e}{0.4}\right)^2 \text{ eV}, \end{aligned} \quad (10)$$

$$\begin{aligned} F_{\varepsilon_c} &\simeq \frac{\sqrt{3}e^3 B' N}{m_e c^2} \frac{2\Gamma_j(1+z)}{4\pi d_L^2} \simeq 1.3 \times 10^4 L_{55}^{3/2} \Gamma_{j,3}^{-3} \\ &\times \theta_p^{1/2} \left(\frac{\epsilon_B}{10^{-5}}\right)^{1/2} \text{ keV cm}^{-2} \text{ s}^{-1} \text{ keV}^{-1} \end{aligned} \quad (11)$$

where $N = [L\Delta t_i / (1+z)] / (\Gamma_j m_p c^2)$. The 1st-order SSC characteristic energy and the SSC peak flux are approximately

$$\begin{aligned} \varepsilon_m^{\text{SC}} &\simeq 4\gamma_m^2 \varepsilon_m \simeq 1.7 L_{55}^{1/2} \Gamma_{j,3}^{-2} \left(\frac{\Delta t_i}{2 \text{ s}}\right)^{-1} \\ &\times \theta_p^{9/2} \left(\frac{\epsilon_B}{10^{-5}}\right)^{1/2} \left(\frac{\epsilon_e}{0.4}\right)^4 \text{ MeV}, \end{aligned} \quad (12)$$

$$\begin{aligned} F_{\varepsilon_c}^{\text{SC}} &\simeq \tau F_{\varepsilon_c} \simeq 3.4 L_{55}^{5/2} \Gamma_{j,3}^{-8} \left(\frac{\Delta t_i}{2 \text{ s}}\right)^{-1} \\ &\times \theta_p^{1/2} \left(\frac{\epsilon_B}{10^{-5}}\right)^{1/2} \text{ keV cm}^{-2} \text{ s}^{-1} \text{ keV}^{-1} \end{aligned} \quad (13)$$

We find that the 1st-order SSC radiation can account for the observed MeV emission of this burst. The emission just below ε_c is suppressed by synchrotron self-absorption effect, and the 2nd-order SSC emission is suppressed by the Klein-Nishina effect.

4. Upscattered Cocoon (UC) emission

Here we derive the observed spectrum of the UC emission as a function of the polar angle θ of the emitting region on the shell (see Figure 1). The spectrum of radiation scattered at an angle θ'_{sc} relative to the direction of the photon beam in the Thomson scattering regime is given by [9, 10, 20]

$$j'_{\varepsilon'}(\theta'_{\text{sc}}) = \frac{3}{2} \sigma_T (1 - \cos \theta'_{\text{sc}}) \int d\gamma N'(\gamma) \int_0^1 dy J'_{\varepsilon'_s}(1-2y+2y^2), \quad (14)$$

where $y = \varepsilon' / [2\gamma^2 \varepsilon'_s (1 - \cos \theta'_{\text{sc}})]$. This is the scattered radiation emissivity in the jet comoving frame, $N'(\gamma)$ is the electron energy spectrum, and $J'_{\varepsilon'_s}$ is the intensity of the seed photons averaged over solid angle, i.e., the mean intensity. The term $\xi \equiv 1 - \cos \theta'_{\text{sc}}$ describes the anisotropy of the spectrum, and this is due to the fact that the IC scattering is strongest for the head-on collisions between electrons and seed photons. This implies that the UC emission in the observer frame is stronger from the high-latitude region of the shell, so that its flux peak lags behind the onset of the synchrotron and SSC emission of the same electrons, which have isotropic energy distribution in the comoving frame of the jet.

In order to concentrate on the time-averaged spectrum including the high-latitude emission, we calculate the flux of the UC emission by neglecting the radial structure of the emitting shell for simplicity. The peak energy and the peak flux of the UC emission are reduced as functions of the angle parameter $q(\theta) \equiv \Gamma_j^2 \theta^2$:

$$\begin{aligned} \varepsilon_m^{\text{UC}} &= 2\gamma_m^2 \varepsilon_{\text{ph}}^{\text{co}} \frac{\xi(\theta)}{1 + \Gamma_j^2 \theta^2} \\ &\simeq 160 \text{ MeV} \left[\frac{4q}{(1+q)^2} \right] \left(\frac{\gamma_m}{400} \right)^2 \left(\frac{\varepsilon_{\text{ph}}^{\text{co}}}{1 \text{ keV}} \right) \quad (15) \\ \varepsilon_m^{\text{UC}} F_{\varepsilon_m}^{\text{UC}} &= 3\tau \gamma_m \gamma_c \varepsilon_{\text{ph}}^{\text{co}} F_{\varepsilon_{\text{ph}}}^{\text{co}} \frac{\xi^2(\theta)}{[1 + \Gamma_j^2 \theta^2]^3} \\ &\simeq 580 \text{ keV cm}^{-2} \text{ s}^{-1} \left[\frac{40q^2}{(1+q)^5} \right] \left(\frac{\tau}{4 \times 10^{-4}} \right) \\ &\times \left(\frac{\gamma_m}{400} \right) \left(\frac{\gamma_c}{400} \right) \left(\frac{\varepsilon_{\text{ph}}^{\text{co}} F_{\varepsilon_{\text{ph}}}^{\text{co}}}{30 \text{ keV cm}^{-2} \text{ s}^{-1}} \right), \end{aligned} \quad (16)$$

where the functions in the brackets $[\]$ both have values of zero at $q = 0$ and $q = \infty$ and have peaks of 1 at $q = 1$ and $\simeq 1.4$ at $q = 2/3$, respectively. This means that the UC flux has a peak at $q \simeq 1$, or $\theta \simeq \Gamma_j^{-1}$,

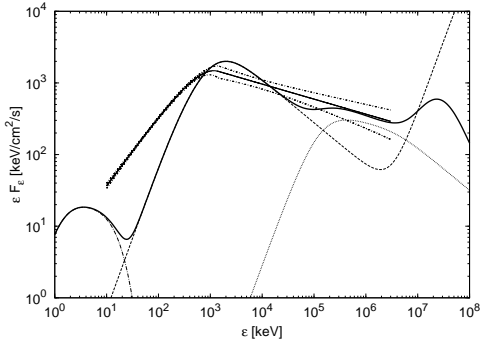


Figure 2: Time-averaged spectrum of the second pulse calculated in the up-scattered cocoon emission model. The 1st-order SSC component plus 2nd-order SSC component without including the Klein-Nishina effect (*dashed line*), the cocoon photospheric emission (*dot-dashed line*), and the UC emission (*dotted line*) are shown. The *thick solid line* represents the combination of these, taking account of the Klein-Nishina effect, which is roughly consistent, at $\varepsilon \gtrsim 1$ MeV, with the Band model spectrum (*thin solid line*) with 95% confidence errors (*dot-short-dashed lines*) (from the LAT/GBM group of *Fermi*). The bump at ~ 30 GeV is so dim as not to be detected. The adopted parameters are listed in equation (17) and (18).

i.e., the peak time of the UC emission lags behind that of the SSC emission on the angular spreading timescale, $\Delta t_i \simeq 2$ s. This is consistent with the observed lag of the GeV emission onset behind the MeV emission peak of the second pulse of GRB 080916C. Here the values of the jet parameters $\tau = 4 \times 10^{-4}$ and $\gamma_m = \gamma_c = 400$ are applicable for the 1st-order SSC emission of the jet being consistent with the observed MeV emission component (see § 2). This indicates that the UC emission of the electrons accelerated in the internal shock of the jet, emitting the observed MeV emission, can naturally explain the observed flux in the GeV range.

If the flux of the cocoon photospheric X-rays is given, i.e., E_c , Γ_c , and r_* , are given, the fluxes of the UC and SSC emission of the jet are determined by the jet parameters L , Γ_j , Δt_i , ϵ_B , and ϵ_e . Since $\Delta t_i \sim 2$ s is roughly given by the observations, and this value is necessary to explain the observed high-energy lag timescale, we have four free parameters. On the other hand, we have four characteristic observables; the peak fluxes and peak photon energies of the SSC component and the UC component. Therefore the jet parameters are expected to be constrained tightly.

Figure 2 shows the result of the time-averaged spectrum of the second pulse for the cocoon parameters

$$E_{c,52} = 1.0, \quad \Gamma_c = 52, \quad r_{*,11} = 2.5, \quad (17)$$

and $\beta = -1.2$. These values satisfy the constraints on the cocoon parameters, equations (3) and (7). This

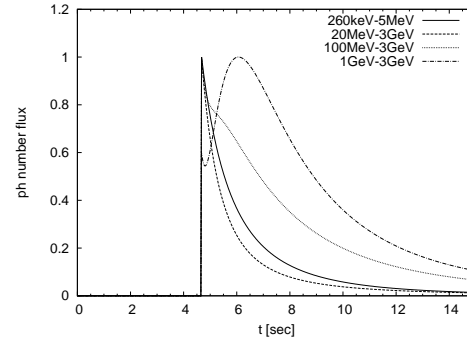


Figure 3: Photon number fluxes of the second pulse in several frequency ranges calculated in the up-scattered cocoon emission model. Each lightcurve is normalized to a peak flux of unity. The peak of the GeV lightcurve is delayed behind that of the MeV lightcurve.

figure shows that our model is roughly consistent with the observed spectrum at $\varepsilon \gtrsim 1$ MeV. The adopted values of the jet parameters are

$$L_{55} = 1.1, \quad \Gamma_{j,3} = 0.93, \quad \Delta t_i = 2.3 \text{ s}, \quad \epsilon_B = 10^{-5}, \quad \epsilon_e = 0.4, \quad (18)$$

and $p = 3.2$. The corresponding values of the optical depth for electron scattering and the characteristic electron Lorentz factors are $\tau = 3.5 \times 10^{-4}$, $\gamma_m = 400$, $\gamma_c = 390$. Figure 3 shows the results of the multi-band lightcurves for the same parameters. Each lightcurve is normalized to a peak flux of unity. This clearly displays the lag of the high-energy emission peak.

5. Discussion

We have discussed a model in which the prompt emission spectrum consists of an MeV component produced by the SSC emission of electrons accelerated in internal shocks in the jet and the high-energy component produced by up-scattering of the cocoon X-rays off the same electrons (UC emission), and we have shown that this model can explain the above three observed properties (i), (ii), and (iii) listed in § 1. The expanding cocoon may become optically thin some time later than the first internal shock of the jet (equation 2), so that the first MeV pulse may not be associated with the UC emission while the second MeV pulse may be associated with it (property (ii)). The UC emission has an anisotropic energy distribution in the comoving frame of the jet so that the observed UC emission is stronger from the higher-latitude region of the shell. This results in the lag of the flux peak of the UC emission behind the MeV emission onset on the angular spreading timescale (property (iii)). Figure 2 shows that the combination of the SSC and UC emission can reproduce the observed high-energy spectral data (property (i)). The UC emission is short-lived

(roughly for $\Delta t_c \simeq 7.5$ s) and may not account for the whole high-energy emission which lasts longer than the MeV emission (property (iv)). It is natural that the high-energy emission in the later times is related to the afterglow. This has been shown by [18]. However, the early portion of the high-energy emission should be the UC emission, because the external shock cannot reproduce the observed steep rise of the flux.

We have focused on GRB 080916C because of its extensive data on the high-energy emission. However our model is generic, and it could apply to other *Fermi*-LAT GRBs with typical parameters $L \simeq 10^{53}$ erg s⁻¹, $\theta_j \simeq 0.1$, and $\Gamma_j \simeq 300$ for which the prompt emission in the soft γ -ray range is produced by the 1st-order SSC radiation of electrons [19]. Some short GRBs might originate from the collapses of the massive stars [21], and thus they could have the delayed UC emission. Even if other short GRBs are produced by the compact star mergers, it might be possible that the jet is accompanied by the delayed disc wind [22] and that the emission from the disc wind is up-scattered by the electrons accelerated in the jet. For either progenitor models, the delayed high-energy emission associated with short GRBs, if any, would provide an interesting tool to approach their origins.

A simple prediction of our model is that prompt emission spectra of some GRBs would have an excess above the Band spectrum around ~ 1 keV due to the cocoon photospheric emission, and this excess should have a different temporal behavior from that of the MeV emission. In addition, we expect GRB 080916C to have had bright synchrotron emission in the optical band, like the "naked-eye" GRB 080319B.

If our model is correct, we can constrain the parameter range for which hadronic effects are important on the high-energy emission of GRBs, and we can also constrain the models of high-energy cosmic ray acceleration. Also, the delay time of the onset of the high-energy emission is directly linked to the optical-thinning time of the expanding cocoon, which constrains the physical parameters of the progenitor star and the cocoon material of GRBs. For GRB 080916C, the stellar radius r_* and the total energy E_c and mass M_c of the cocoon are constrained to be $0.3 < E_{c,52}^{-2} (M_c/10^{-4} M_\odot)^{2.5} \lesssim 0.9$ and $r_{*,11} \gtrsim 0.8 E_{c,52}^5 (M_c/10^{-4} M_\odot)^{-3}$ (see equations 3 and 7). The cocoon energy and the cocoon mass come from the jet energy released within the star and the stellar mass swept by the jet, respectively. These constraints therefore provide potential tools for investigating the structure of the progenitor star just before the explosion, as well as the physical conditions of the jet propagating inside the stellar envelope through either analytical [12, 13] or numerical [14, 15] approaches.

Acknowledgments

We acknowledge NASA NNX09AT72G, NASA NNX08AL40G, and NSF PHY-0757155 for partial support. XFW was supported by the National Natural Science Foundation of China (grants 10503012, 10621303, and 10633040), National Basic Research Program of China (973 Program 2009CB824800), and the Special Foundation for the Authors of National Excellent Doctorial Dissertations of P. R. China by Chinese Academy of Sciences.

References

- [1] Atwood, W. B., et al. 2009, ApJ, 697, 1071
- [2] Mészáros, P. 2006, Rep. Prog. Phys., 69, 2259
- [3] Falcone, A. D., et al. 2008, GRB section of the white paper on the status and future of ground-based TeV gamma-ray astronomy (arXiv:0810.0520)
- [4] Abdo, A. A., et al. 2009a, Science, 323, 1688
- [5] Abdo, A. A., et al. 2009b, ApJ, 706, L138
- [6] Asano, K., Inoue, S., & Mészáros, P. 2009, ApJ, 699, 953
- [7] Razzaque, S., Dermer, C., & Finke, J. D. 2009, arXiv:0908.0513
- [8] Wang, X. Y., Li, Z., Dai, Z. G., & Mészáros, P. 2009, ApJ, 698, L98
- [9] Wang, X. Y., & Mészáros, P. 2006, ApJ, 643, L95
- [10] Fan Y. Z., Piran, T., Narayan, R., & Wei, D. M. 2008, MNRAS, 384, 1483
- [11] Beloborodov, A. M. 2005, ApJ, 618, L13
- [12] Mészáros, P., & Rees, M. J. 2001, ApJ, 556, L37
- [13] Matzner, C. D. 2003, MNRAS, 345, 575
- [14] Zhang, W., Woosley, S., & MacFadyen, A. I. 2003, ApJ, 586, 356
- [15] Morsony, B. J., Lazzati, D., & Begelman, M. C. 2007, ApJ, 665, 569
- [16] Ramirez-Ruiz, E., Celloti, A., & Rees, M. J. 2002, MNRAS, 337, 1349
- [17] Pe'er, A., Mészáros, P., & Rees, M. J. 2006, ApJ, 652, 482
- [18] Kumar, P., & Barniol Duran, R. 2009, MNRAS in press (arXiv:0905.2417)
- [19] Toma, K., Wu, X.-F., & Mészáros, P. 2009, ApJ, 707, 1404
- [20] Brunetti, G. 2001, Astropart. Phys., 13, 107
- [21] Zhang, B., et al. 2009, ApJ, 703, 1696
- [22] Metzger, B. D., Piro, A. L., & Quataert, E. 2008, MNRAS, 390, 781